ORIGINAL

Evolution of the Parnaíba Delta (NE Brazil) during the late Holocene

**Agata Szczygielski · Karl Stattegger · Klaus Schwarzer ·
André Giskard Aquino da Silva · Helenice Vital ·
Juliane Koenig**

Abstract Sedimentary processes and the evolution of the wave- and tide-dominated, asymmetric Parnaíba Delta during the late Holocene were investigated based on geochemical and sedimentological analyses of sediment cores collected in 2010, as well as satellite images and historical maps. This is a rare case of pristine deltas essentially unaffected by human activities worldwide. The lowermost part of the main Parnaíba River distributary exhibits several low-sinuosity bends and several anastomosing bifurcation patterns in the east, whereas three NW–SE-oriented tidal channels drain a large mangrove area in the west. Dating of various materials in sediment cores from the tidal flats, tidal channels and supratidal marshes revealed that the oldest sediment (4,853 to 4,228 cal. years BP) is paleo-mangrove soil from the main river distributary. Present-day mangroves and marshes up to 200 years old exhibit high sedimentation rates reaching 3.4 cm/year. The asymmetry of the delta is explained not only by the wind- and wave-induced westward-directed longshore drift but also by neotectonic processes, as revealed by satellite images. Faulting and eastward tilting may have triggered delta lobe switching from west to east. This would explain the erosional character and unusual updrift orientation of the main river-mouth channel. Consistent with existing knowledge on mangrove ecosystems worldwide, sediment carbon and nitrogen signatures lie in the range of freshwater or marine dissolved organic carbon and C_3 terrestrial plants. In the western tidal channels, the low C_{org}/N_{tot} ratios (16–21) of young mangrove soil (deposited in the last 16 years) reflect a stronger influence of marine plants compared to older mangroves (1,390–1,525 cal. years BP; ratios of 20–37). Thus, there would have been a greater influence of the Parnaíba River on tidal-channel sedimentology 1,400 to 1,500 years ago, entailing a natural connection between the present-day tidal channels and the river in ancient times, which was abandoned later during delta lobe switching. This is substantiated by historical maps that indeed show this connection between the main distributary and the tidal-channel system.

A. Szczygielski (✉) · K. Stattegger · K. Schwarzer ·
A. G. A. da Silva · J. Koenig
Institute of Geosciences, Department of Sedimentology, Coastal and Continental Shelf Research, University of Kiel, Otto-Hahn-Platz 1, 24118 Kiel, Germany
e-mail: asz@gpi.uni-kiel.de

H. Vital
Universidade Federal do Rio Grande do Norte (UFRN),
P.O. Box 1596, 59078-970 Natal, RN, Brazil

Introduction

Most modern large delta systems are impacted by multiple threats, including the agricultural usage of coastal wetlands, mangrove clearance (e.g., the Mekong), water diversion schemes, upstream sediment retention by damming (e.g., the São Francisco and the Yangtze), and the extraction of water and hydrocarbons (e.g., the Niger). Human activities result in increasing subsidence, marine inundation and coastal erosion, modifying and deteriorating delta morphology and posing ever-increasing challenges for coastal restoration (e.g., Syvitski and Saito 2007; Jaffe et al. 2007; Syvitski et al. 2009; Lo et al. 2014). Indeed, today there exist only rare cases of deltas essentially unaffected by human activities worldwide.

The NE regions of Brazil comprise areas of low population density and well-preserved ecosystems (Szlafsztein 2003). The Parnaíba River is the largest river system between the São Francisco and Amazon rivers. The river was dammed in the 1970s (Companhia Hidro Elétrica do São Francisco, CHESF 2014) 630 km upstream, forming a 350 km² reservoir. However, satellite images available since the 1970s (LANDSAT 2/5TM_1975-2003) do not show major changes in the river's wave- and tide-dominated delta morphology (Fig. 1). Indeed, the river catchment–coast continuum exhibits

Fig. 1 Satellite image of the Parnaíba Delta (LANDSAT 5TM_2003) with core locations and morphological elements: *1* ebb delta, *2* main ebb channels, *3* inlets with back-barrier channel system, *4* mangroves, *5* transgressive dune fields, *6* partly inactive dune field
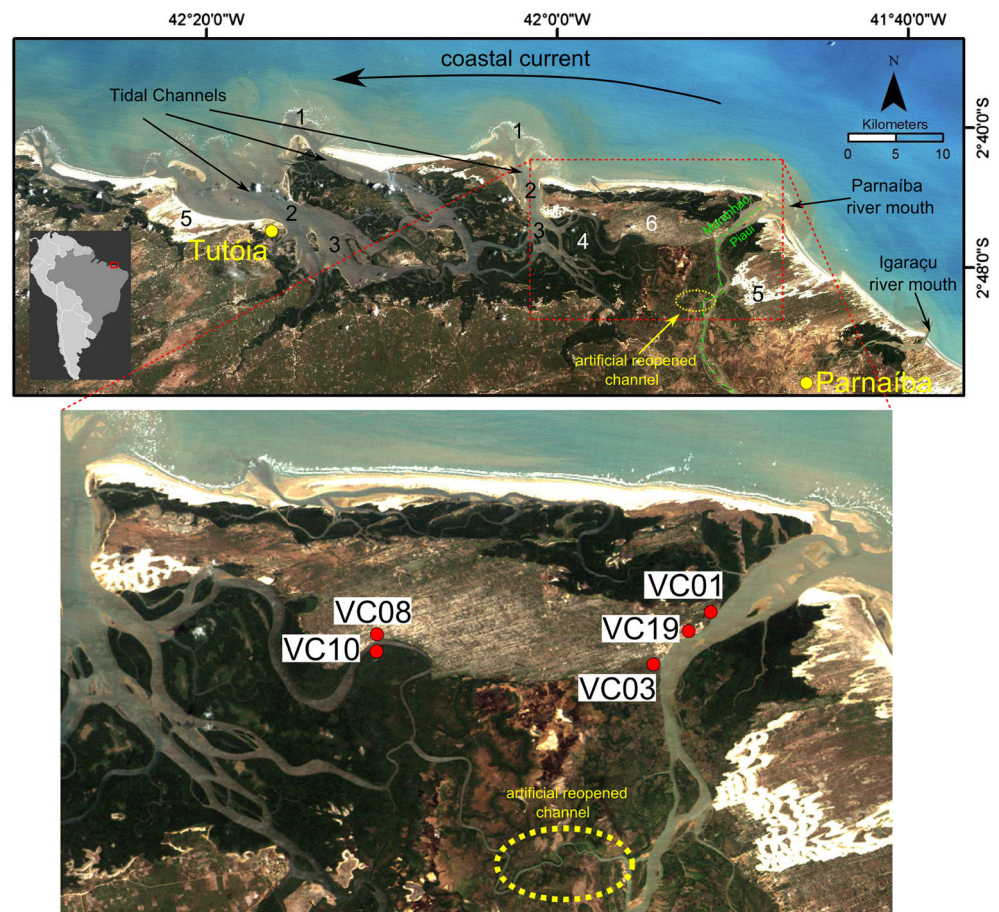
only minor anthropogenic influences. Such pristine delta settings are becoming increasingly rare archives for research on natural delta evolution in recent times.

Within this general framework, previous work in NE Brazil has focused primarily on the structural geology of the Parnaíba Basin and the Marajó Basin, the drainage system of the Sobradinho platform (e.g., Arora et al. 1999; Costa et al. 2002; Almeida-Filho et al. 2009), and Holocene sea-level changes (e.g., Bezerra et al. 2003; Angulo et al. 2006; Caldas et al. 2006a, 2006b; Irion et al. 2012; for overview of earlier work see, for example, Knoppers et al. 1999). The Parnaíba Delta has not been a focus of intense research to date. Nevertheless, already Suguio and Martin (1981) drew attention to the Holocene evolution of this and other deltas along the Brazilian coast, distinguishing between (quote) "an older phase related to a fluvial-dominated, constructive, intralagoonal delta and a newer one related to a wave-dominated, destructive delta that is still active today".

The objective of the present study, based on two field campaigns conducted in 2010, was to explore the late Holocene evolution of the essentially pristine Parnaíba Delta in more detail. For this purpose, geochemical and sedimentological analyses of deltaic deposits were carried out on sediment cores collected from tidal flats, tidal channels and

supratidal marshes. Those data are interpreted in combination with satellite images and historical maps.

Physical setting

Overview

On the northeast Brazilian coast, the Parnaíba Delta straddles the state of Piauí to the east and the state of Maranhão to the west (Fig. 1). The Parnaíba River originates in the East Brazilian highlands and flows north, forming the boundary between these states along most of its course. The drainage basin covers 333, 056 km^2 (Agencia Nacional de Águas, ANA 2013), and forms part of the Parnaíba sedimentary basin to the south and the Barreirinha Basin to the north (Dominguez 2009). The river is 1,400 km long (ANA 2013), and discharges into the Atlantic Ocean where it forms a wave-dominated and tidally influenced delta (Wright and Coleman 1973; Bhattacharya and Giosan 2003). The subaerial part of the Parnaíba Delta itself extends over 2,700 km^2 (Labohidro 1999), and comprises numerous islands associated with a complex channel network. The delta is larger than that of the São Francisco, but smaller than the Amazon Delta (Table 1). It is asymmetric in shape. River

Table 1 Delta parameters of Parnaíba, São Francisco and Amazon rivers in NE Brazil

Delta	Area of subaerial delta plain (km^2)	Average discharge (m^3/s)	Hydrodynamic forcing and type of sediment dispersal system (after Walsh and Nittrouer 2004)
Parnaíba	2,700 (Labohidro 1999)	1,272 (Marques et al. 2004)	Wave, tides, proximal-accumulation dominated
São Francisco	800 (Traini et al. 2012)	2,000 (Bittencourt et al. 2007)	Waves, canyon captured
Amazon	467,100 (Syvitski and Saito 2007)	173,000 (Martinez et al. 2009)	Tides, subaqueous delta clinoform

discharge is exposed to SW-directed waves, W–NW-directed coastal currents (north Brazil current), and mesotidal forcing.

Two types of coasts dominate the Parnaíba Delta region (Fig. 1). The eastern part of the delta consists of an actively migrating coastal dune field, which covers mangrove forests and older, partly vegetated dune fields. It is enclosed by the two distributaries of the Parnaíba Delta: the larger Parnaíba River to the west, and the smaller Igaraçu River to the south-east. Beaches up to 200 m wide and prograding barriers characterize the coastal geomorphology.

West of the river mouth, the coast is dominated by tidal channels associated with estuarine-lagoonal conditions. Deflation plains are preserved in between mangrove-dominated islands and deltaic plains. In addition to the dune field and narrow beaches, several sand spits occur. Further inland, dune systems are common (Hesp et al. 2009). Virgin forests and huge mudflats occur throughout the delta. A particular feature is the artificial reopening of a naturally abandoned channel in about 1960 (oral communication from local farmers); this channel connects the river and the tidal-channel system as a local waterway (Fig. 1).

Hydrology and currents

The Parnaíba Delta is situated close to the equator, and the regional climate is influenced by the Intertropical Convergence Zone, El Nino, and South Atlantic anticyclone (Nimer 1979). There are marked seasonal variations in rainfall. From August to December, semiarid conditions with diminished riverine discharge prevail. From December to April, winds from the northeast generate swell waves, whereas the southeast trade winds dominate for the remainder of the year. This is an open, wave-dominated mesotidal coast with a semidiurnal tidal regime (Hesp et al. 2009). Tides range from 1.1 m during neap tide to 3.3 m during spring tide (Luís Correia Harbor, Igaraçu river mouth). Longshore currents along the northeastern Brazilian coast, including off the Parnaíba Delta, are directed from east to west (Fig. 1).

Materials and methods

During two field campaigns in March and November 2010, 18 vibro-cores up to 320 cm in length (technique after Lanesky

et al. 1979) and 21 surface samples were taken mostly during low tide. Five cores (Table 2) from the intertidal zone were examined in detail based on the setting, internal structure and lithology. Core VC01 was taken from a swamp close to the river mouth, core VC03 from young mangrove soil close to the river, and core VC19 from old mangrove soil exposed along the river bank. Cores VC08 and VC10 were taken from the western tidal channels of the delta (Figs. 1 and 2).

The structural and lithological characteristics were described and documented by means of photographs. For cores VC03, VC08 and VC01, X-ray radiographs enabled more detailed examination. Based on those preliminary observations, distinct layers were sampled for determination of grain size, total organic carbon and total nitrogen contents, and age based on ^{210}Pb and ^{14}C measurements. Additionally, old maps (Heck 1842; Walle 1910) were compared with more recent satellite images to interpret changes in the channel network and river course.

Laser granulometry was used for the grain-size analyses of clay (grain size <0.002 mm) to coarse sand (grain size <2 mm), by means of a LS 13 320 Particle Size Analyzer (Beckman Coulter, manual version 2011). The description of sediment composition follows the classification scheme of Folk (1954). The samples were taken in 2- to 10-cm steps, depending on sediment layers and internal structure. Fine-grained and sandy layers, alternating at mm to cm scales, were sampled separately. Ages and sedimentation rates were assessed by means of ^{210}Pb analyses of fine-grained samples from various layers, performed at the GEOMAR and the Leibniz Laboratory for Radiometric Dating and Isotope Research in Kiel.

Sedimentary organic matter sources were evaluated based on organic carbon and nitrogen measurements on powdered bulk sediments, using a Carlo Erba Element Analyzer NA-1500. Moreover, ^{12}C and ^{13}C isotopes were analyzed in bulk samples with a Finnigan MAT 252 isotope mass spectrometer at the Institute for Biogeochemistry and Marine Chemistry (IfBM) in Hamburg.

The radiocarbon ages of wood and plant fragments of cores VC01 (241 cm), VC03 (248–252 cm), VC08 (196–197 cm) and VC19 (100 cm) were determined using the accelerator mass spectrometry (AMS) system Tandetron 4130 of the Leibniz Laboratory (cf. Stuiver and Polach 1977). Ages were determined also for one piece of wood (code 1703102B1, 2–4

Table 2 Geographical locations and settings of the cores used in this study

Core code: original (working)	Date	Latitude S	Longitude W	Recovery length (cm)	Coastal environment
VC-IC-01 (VC01)	March 2010	2°45.735′	41°50.288′	274	Marsh at main river mouth
VC03-05112010 (VC03)	5 Nov. 2010	2°46.418′	41°51.064′	320	Mangrove fringe at main river mouth
VC19-11112010 (VC19)	11 Nov. 2010	2°45.908′	41°50.440′	110	Old mangrove soil at main river-mouth embankment
VC08-06112010 (VC08)	6 Nov. 2010	2°46.035′	41°56.079′	320	Embankment at tidal channel
VC10-06112010 (VC10)	6 Nov. 2010	2°46.103′	41°56.017′	56	Mangrove forest at tidal channel

m water depth) and a shell fragment (1703102B2, 6 m water depth) from the steep flank of the river bank very close to core VC19. Radiocarbon ages were converted into calendar years BP with the CALIB 7.0 software (Reimer et al. 2013; Table 3).

Radionuclide measurements were performed on dried, grinded bulk samples of cores VC01, VC03, VC08 and VC10 at the GEOMAR and the Leibniz Laboratory. In addition to total ^{210}Pb (46.5 keV), ^{137}Cs (662 keV) and ^{214}Pb (352 keV) were measured (cf. gamma peaks at 46.5, 362 and 661 keV, respectively).

Results

Core VC01: high marsh at main river mouth

Core VC01 was taken 500 m downstream of core VC19 and 5 km inland from the river mouth on a marsh regularly flooded during spring tides. Two units can be distinguished based on their lithologies (Table 4). These units 1 and 2 have no visible internal structures (e.g., lamination or bioturbation), but laminated bedding is observed in the transition zone between the units (Figs. 3 and 4). *Unit 1* is composed of mud down to a core depth of 114 cm. In the transition zone, the grain size changes gradually to sandy mud and in the bottommost part to muddy sand. The X-ray images show some deformed to subparallel lamination from 162 to 171 cm (Fig. 4). *Unit 2* is composed mostly of moderately well-sorted medium sand, with no internal structures.

N_{tot} contents fluctuate around 0.2% from the core top to a depth of 90 cm, below which they decrease gradually to 0.03% at 179 cm (Fig. 5). C_{org} contents increase downcore to a depth of 90 cm—from 3.40% to 5.16%—and then decrease to 0.92% at 179 cm. C_{org}/N_{tot} ratios vary strongly between 15.34 and 33.46. $\delta^{13}C$ values decrease from –21.08‰ at the core top to –27.1‰ at 60 cm depth, and then increase slightly toward the base of the core.

There were substantial errors in ^{210}Pb$_{excess}$ activity (±2.96 to ±7.70 Bq/kg), so that it was not possible to create a reliable age model for core VC01. The radiocarbon dating of a piece of wood from a core depth of 241 cm yielded an age range of 217–143 cal. years BP.

Core VC03: mangrove fringe at main river mouth

Core VC03 was taken close to the main river mouth channel and approx. 6 km from the river mouth near the northern end of a mangrove fringe adjacent to a dune field (Figs. 1 and 2). Three units can be distinguished based on changes in lithology and/or internal structure (Table 4). At 23 cm depth, a sharp boundary separates units 1 and 2 (Fig. 3). Unit 2 is separated from unit 3 by a subtle change in internal structure at 236 cm.

Unit 1 is composed of sandy mud to muddy sand, without visible internal structure (Figs. 3 and 4). *Unit 2* is composed mostly of alternating mud and sandy mud layers. The X-ray images show fine laminations (Fig. 4), with bioturbation structures in the upper part (60–94 cm). Several pieces of wood occur in the sediment of this unit. In *unit 3*, sandy mud layers alternate with thin layers of muddy sand and layers composed only of sand. The sandy mud layers dominate. Lenticular bedding is the main structure. Due to disturbance during core extraction, it was difficult to recognize

Fig. 2 Photographs of core locations and coastal environments

Table 3 Radiocarbon ages and calendar years BP calibrated with the CALIB 7.0 software using IntCal13 (Stuvier and Polach 1977; Reimer et al. 2013); elevation is relative to mean sea level; *WD* water depth, corrected *pMC* percent of modern (1950) carbon corrected for fractionation using the ^{13}C measurement

Lab. code	Core, sample	Material	Core depth (cm)	Elevation (m)	Corrected pMC	δ^{13}C (‰)	AMS ^{14}C age (years BP)	Calibrated age (years BP, 2σ)
KIA44875	VC01	Plant fragment	241	+1.1	97.58±0.30	−27.65±0.08	195±25	217–143
KIA44876	VC03	Plant fragment	248–252	−0.7	98.52±0.30	−27.59±0.12	120±25	148–54
KIA45540	VC19	Piece of wood	100	+0.4	61.76±0.24	−29.09±0.18	3,870±30	4,413–4,228
KIA43275	1703102B1 (near VC19)	Piece of wood	2–4 m WD	<0.0	59.83±0.22	−23.46±0.13	4,125±30	4,726–4,530
KIA43276	1703102B2 (near VC19)	Shell fragment	6 m WD	<0.0	59.14±0.23	−4.92±0.35	4,220±30	4,853–4,801
KIA44877	VC08	Piece of wood	196–197	−0.8	82.39±0.25	−32.82±0.26	1,555±25	1,525–1,390

bioturbation structures. There are still several very thin organic layers, but roots can no longer be observed. The sediment composition fluctuates between sandy mud, muddy sand and sand (Fig. 3). The sand content in the sandy layers increases downcore, from approx. 1% at 25 cm depth to 85% at the bottom of the core (308 cm).

In core VC03, N_{tot} contents vary from 0.03–0.13%, and C_{org} contents from 0.86–2.47% (Fig. 5). δ^{13}C values range between −26.19 and −23.91‰. There are no measurable differences in the ranges between the units within the core.

^{210}Pb$_{excess}$ activity varies throughout the core (between 1.51 and 8.26 Bq/kg). The radiocarbon age range of a piece of wood from 248–252 cm depth (unit 3) is 148–54 cal. years BP.

Core VC19: old mangrove soil at main river mouth

Core VC19 (110 cm length) was taken from old mangrove soil along the eroding river-channel banks, 1.5 km downstream of core VC03 (Fig. 1). This old mangrove soil comprised only one unit, characterized by sandy mud (Fig. 3). At the core top (1–10 cm) and bottom (107 cm), sand contents are relatively high (up to 78%). The core is permeated by roots, and changes in color are common.

N_{tot} contents increase from 0.03% at the core top to 0.10% at 60 cm depth, and then decrease to 0.09% at 100 cm depth. C_{org} contents vary between 1.69 and 2.92%, with the exception of a high value of 4.24% recorded at 20 cm. δ^{13}C values range between −26.99 and −25.61‰.

A piece of wood taken at 1 m core depth has an age range of 4,413–4,228 cal. years BP. Very close to the VC19 coring site, divers collected samples from slabs of the lower part of the mangrove soil that had slid down the river bank. These yielded ages of 4,726–4,530 cal. years BP (piece of wood) at 2–4 m, and 4,853–4,801 cal. years BP (shell fragment) at 6 m water depth.

Core VC08: tidal-channel embankment

Core VC08 was taken on an eroding bank of the cut side of a meandering and generally E–W-trending tidal channel. In the seaward direction, the same dune field that is located north of core VC03 is present (Fig. 1). Changes in lithology and internal structure were observed throughout the core (Figs. 3 and 4), which can be subdivided into three units (Table 4). Between units 1 and 2, a sharp boundary is formed by a 2 mm thick layer of very fine gravel. Units 2 and 3 are separated by subtle changes in internal structure and lithology (Fig. 3).

Unit 1 is composed of finely laminated (mm) mud to muddy sand down to a depth of 52.5 cm. Only subtle differences in sediment composition are observed between the individual laminae (Fig. 4). Bioturbation structures occur in the lower parts (52.5–72.5 cm; Fig. 4). In the upper part (0–7 cm), the lithology is a mixture of core sediment and the surrounding surface material. For this reason, the structure is undefined.

In *unit 2*, well-sorted fine sand layers with thicknesses of 1–10 cm alternate with thinner (1 mm to ~2 cm thick) mud layers. Unit 2 features interlayered sand–mud bedding with

Table 4 Description of cores VC01, VC03 and VC08

Unit, zone	Depth interval (cm)	Description
Core VC01		
Unit 1	0–114	Mud to sandy mud, without structure
TZ	114–180	Transition zone
Unit 2	180–274	Sandy mud, muddy sand, sand, without structure
Core VC03		
Unit 1	0–23	Sandy mud to muddy sand, no internal structure
Unit 2	23–237	Mud and sandy mud, fine lamination (mm)
Unit 3	237–320	Sandy mud, muddy sand, sand, lenticular bedding
Core VC08		
Unit 1	0–72.5	Mud to muddy sand, lamination (mm), bioturbation
Unit 2	72.5–220	Fine sand, mud, flaser bedding
Unit 3	220–320	Sand, cross-bedding

Fig. 3 Core logs depicting clay, silt, sand contents (wet vol%), sedimentary structures, and radiocarbon datings
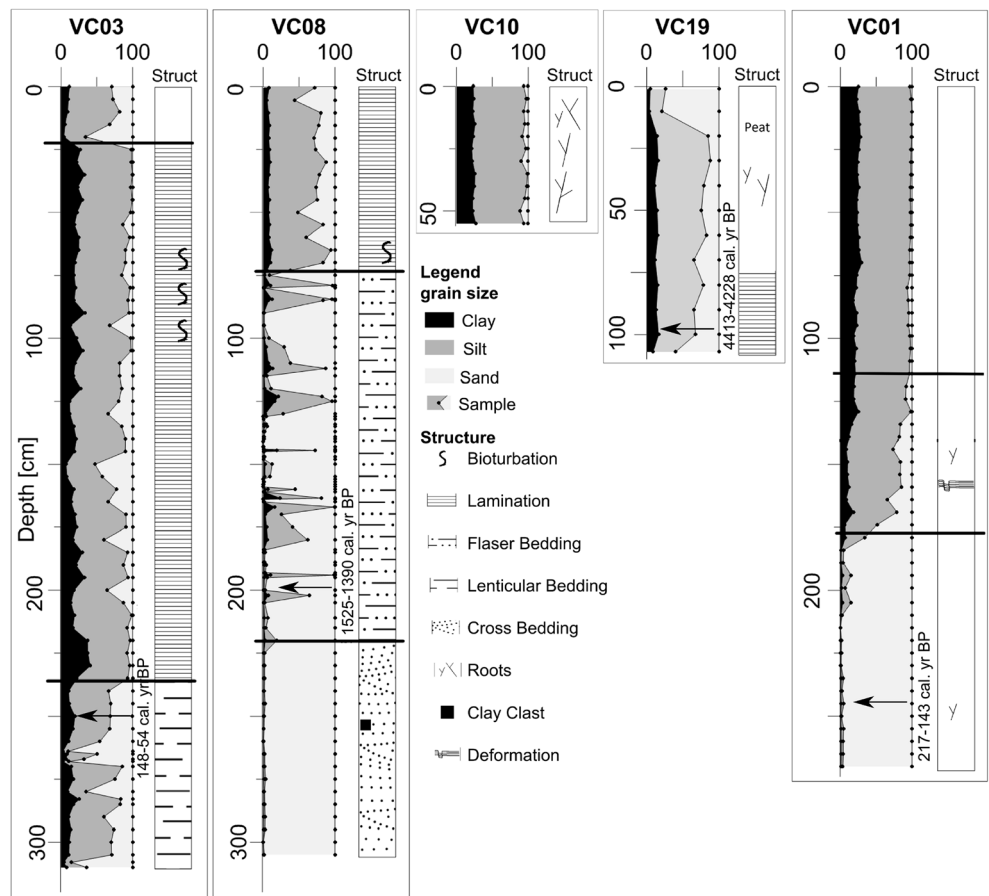
variable thicknesses of the mud and muddy sand layers (Fig. 4). Flaser bedding is dominant. Mud streaks are

preserved at thicknesses of <1 mm to several cm, and the clay contents reach 23%. In some sections, sand layers dominate.

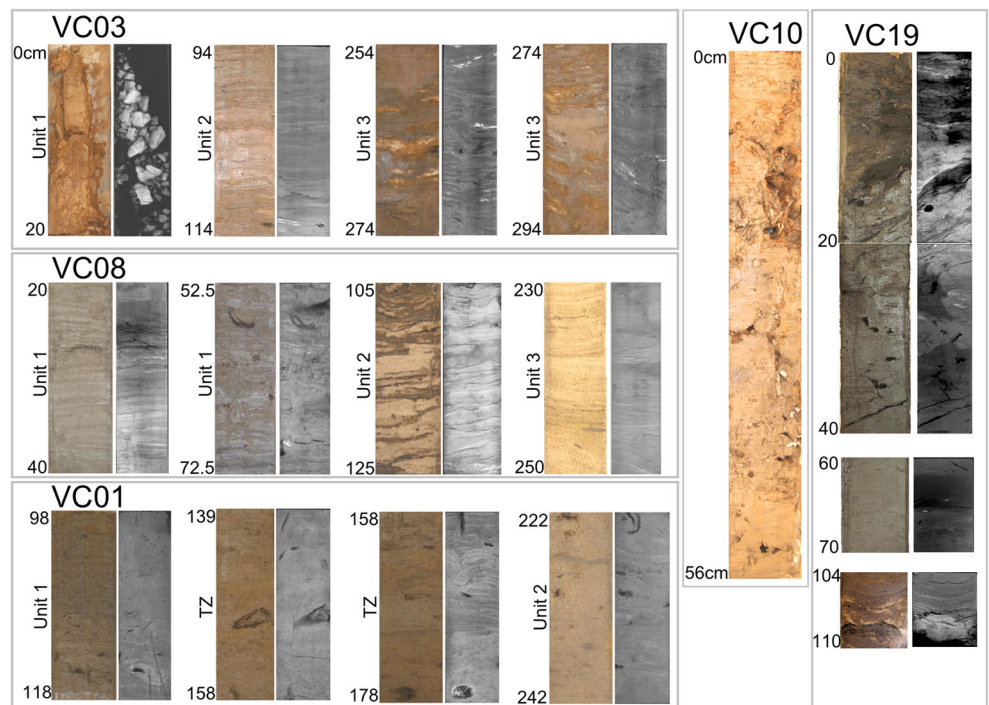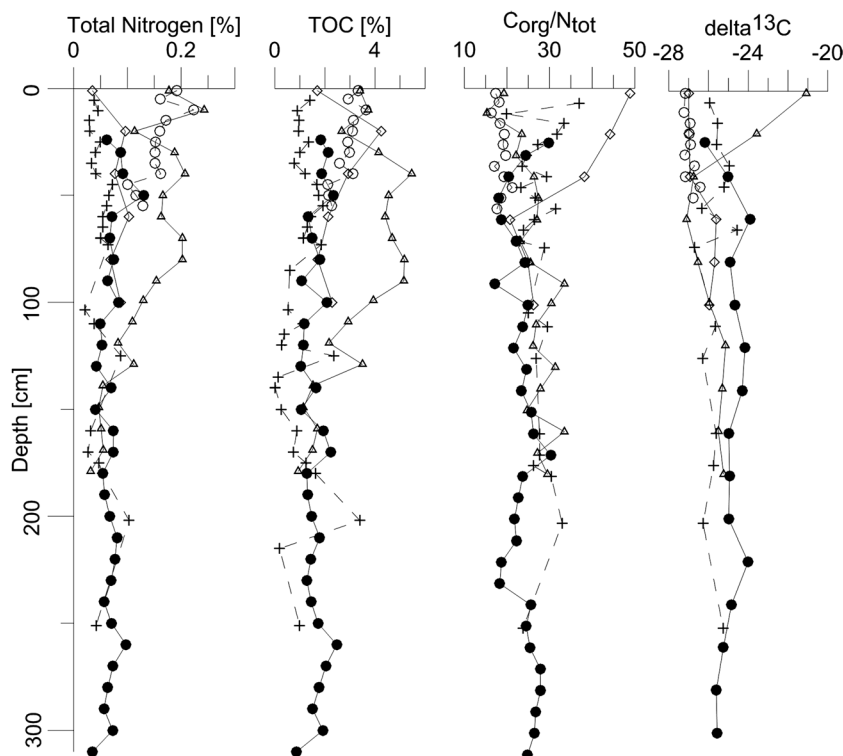**Fig. 4** Core photographs (*left*) and X-ray radiographs (*right*)

Fig. 5 Total nitrogen (N_{tot}) and TOC (total organic carbon, C_{org}) contents, and $\delta^{13}C$ values of the five cores. Δ = VC01, ● = VC03, $\diamond$ = VC19, + = VC08, ○ = VC10

These are either truncated or concordantly overlain by very thin (~1 mm) mud layers (72.5–95, 130–165 and 180–220 cm core depth). In other sections, thin mud layers dominate and are cut by very thin sand layers (95–130 and 165–280 cm). At 152.5 and 162.5 cm, a 1 cm thick burrow filled with sand crosses muddy layers. From 220 cm (*unit 3*) downward, the flaser bedding structure disappears completely, and cross-bedded, very well-sorted fine sand forms the base of the core (Fig. 4). On top (220–234 cm), the sand features parallel lamination, whereas cross-lamination is observed from 234 cm to the bottom. The dip angles range from ca. 1–30°.

High C_{org}/N_{tot} ratios reflect low N_{tot} contents of 0.02–0.10%. In unit 1 the C_{org}/N_{tot} ratios range from 19.84 to 33.35, and in unit 2 from 24.98 to 32.92 (Fig. 5). There are no recognizable differences in $\delta^{13}C$ values between these two units, with values ranging from –26.70 to –24.55‰.

In core VC08, 15 samples from unit 1 and two samples (84–86 and 126.5–129 cm) from unit 2 show no $^{210}Pb_{excess}$ activity, and ^{137}Cs could not be detected. Radiocarbon dating of a piece of wood found at 196–197 cm depth yielded an age range of 1,525–1,390 cal. years BP. There is no age dating of unit 3, because this unit consists of well-sorted fine sand without plant or shell remnants.

Core VC10: mangrove forest at tidal channel

Core VC10 was taken from poorly consolidated sediments of a mangrove forest on the accretion side of the channel bend just opposite of the location of core VC08. It comprises only

one unit along its whole length (56 cm; Fig. 3). The entire core is penetrated by numerous roots, preventing the preparation of X-ray radiographs. The sediment consists largely of mud to sandy mud (Fig. 4).

N_{tot} contents vary over a narrow range of 0.10–0.23% (Fig. 5). C_{org} contents fluctuate from 3–4% in the upper 30 cm, to 2–3% at 30–55 cm. C_{tot}/N_{tot} ratios vary around 20. Compared to core VC08, $\delta^{13}C$ values span a slightly lower range from –27.23 to –26.42‰.

$^{210}Pb_{excess}$ activity decreases progressively from 43.87 to 23.93 Bq/kg from the core top to the bottom. Based on this distinct trend, and assuming that sediment accumulation has been more or less constant, an age of 16 years was calculated for the depth of 55 cm, corresponding to an accumulation rate of 3.4 cm per year.

Discussion

Paleo-environmental interpretation

The sediments of core VC01, retrieved from the high-marsh surface close to the main Parnaíba distributary, differ in structure and lithology from the other cores. The low sand content (0.11–6.67%) in unit 1 indicates low flow velocities during deposition. By contrast, the sandy composition of unit 2, comprising up to 20% coarse sand, indicates higher flow velocities during deposition, possibly related to both fluvial

and tidal conditions. This agrees with the position of the core close to the river channel, which is regularly inundated at spring tide. The river flow and tidal currents seem to have been more intense in the past when the lower sandy unit was deposited. Subsequently, due to river incision and/or sediment accretion, the core site became more frequently inundated by the tides, leading to the deposition of the muddy tidal/ marsh sediments of the unit 1. Although it was not possible to create an age model, the upper part of unit 1 (0 to ~140 cm) most probably accumulated over the last 150 years because there is a determinable positive $^{210}Pb_{excess}$ activity (Nittrouer et al. 1979; Zaborska et al. 2007). According to a radiocarbon age close to 200 years, the lower fluvial unit is slightly older.

The sedimentary facies of units 1 to 3 in core VC03 (sandy mud to mud) suggest deposition on mudflats and sand flats. The lithology and sedimentary structures of unit 1 (no discernible structures) and unit 3 (lenticular bedding) indicate that both were deposited in a fluvial-tidal environment featuring higher energy conditions compared to the finer-grained laminated sediments of unit 2 (cf. Reineck and Singh 1975; Fan 2012; Flemming 2012). Due to large errors in $^{210}Pb_{excess}$ (cf. above), it was not possible to construct a reliable age model. Nevertheless, the deposit is probably younger than 150 years because there is still determinable activity of $^{210}Pb_{excess}$. This young age is supported by the radiocarbon dating of a plant fragment (148–54 cal. years BP).

The sediment of core VC19 is composed of old mangrove soil. The higher sand content (up to 78%) in this core, as compared to that of core VC10 (up to 11%), may be an indicator of deeper water over the tidal flat during deposition (cf. Walsh and Nittrouer 2004). Estimates of depositional rates using ^{210}Pb measurements have not been performed because radiocarbon dating yielded ages exceeding 4,000 years at 1 m depth. The piece of wood (2–4 m water depth) and the shell fragment (6 m water depth) in slabs that slid down from the river bank close to core VC19 yielded ages of 4,853 to 4,530 cal. years BP. This indicates that they belong to the same generation of mangrove forest.

The lithology of unit 1 in core VC08 corresponds to sandy mud facies commonly found around mid-tide level (cf. Walsh and Nittrouer 2004). The mud is laminated (upper 52.5 cm) or homogenized due to bioturbation (52.5–72.5 cm). For mangrove settings, lamination is commonly associated with higher accumulation rates, and bioturbation with lower accumulation rates (e.g., Frey et al. 1989; Alexander et al. 1991). The conditions around the coring site (i.e., an intertidal zone with freshwater input from the hinterland), the location close to the present-day mangrove forests, and the presence of roots confirm that the sediment comprising unit 1 is composed of old mangrove soil. Because of the absence of any determinable $^{210}Pb_{excess}$ activity, the sediment was most likely deposited more than 150 years ago (cf. Nittrouer et al. 1979; Zaborska et al. 2007).

The flaser bedding and the lithology of unit 2 resemble those of tidal flat sequences (Reineck and Singh 1975). The fine-grained muddy sediments intercalated within sandy layers imply an availability of both sand and mud, and a periodic change of current velocities. At spring tide, higher-velocity flood currents may have transported sand from barrier beaches and inlets to the landward-extending tidal flats, whereas the fine-grained layers may have originated from mud flats during the ebb phase or periods of lower flow velocities around neap tides (Reineck and Singh 1975). In unit 3, cross-bedding is the main sedimentary structure. At larger scales, this bedding structure is associated with subaqueous dunes in tidal channels, or with intertidal dunes occurring on the outer tips of flood ramps near tidal inlets (Flemming 2012), whereas smaller-scale cross-bedding occurs widespread on sand flats in association with current ripples (Reineck and Singh 1975). Such bedding structures have also been described from intertidal point bars composed of fine to coarse sand (Reineck and Singh 1975). Flemming (2012) reported similar deposits composed of horizontally laminated beds occurring along the margins of larger and deeper channels. In the present case, however, the cross-bedding was more likely formed by small subaqueous dunes in a tidal channel.

The sediment of core VC10 consists of young mangrove soil. The calculated age of 16 years, with accumulation rates of 3.4 cm/year, agree well with sediment accumulation rates of 4.4±2.8 cm/year found around mid-tide levels in mesotidal environments in the tropical Gulf of Papua (Walsh and Nittrouer 2004), and also with the generally high sedimentation and accumulation rates in mangrove ecosystems in general (Jennerjahn and Ittekkot 2002).

The sediment composition of the cores thus indicates substantial changes in the depositional conditions in the course of delta progradation, and that tidal forcing has been an important factor in the recent past. The sediment cores differ markedly in their lithology, the majority of sedimentary structures appearing to be tide-generated at a variety of water depths (as described by, for example, Reineck and Singh 1975; Schäfer 2005; Fan 2012), whereas fluvial deposits are observed at the base of core VC01. Generally, tidal flat environments display a shoreward-fining grain-size gradient (e.g., Bartholomä and Flemming 2007), which is also recognizable in the available sediment cores. Tidal deposition is not discussed in greater detail here because data on factors such as availability of sediment and water velocity are not available. However, tidal currents clearly influenced deposition in tidal channels and also in tidally influenced sections of the river (cores VC03 and VC19). Although tidal deposits were observed in both delta lobes, it is only in the eastern lobe (core VC01) that tidal influence was also observed at the transition from the fluvial to the estuarine domain.

Historical change in delta morphology

The configuration of a delta is controlled by various parameters such as the coastal morphology, the configuration of the coastline, the slope gradient of the delta front, the direction and intensity of waves, the efficiency of sediment transport on the shelf relative to sediment transport by river distributaries, and tidal forcing (Reineck and Singh 1975; Woodroffe 2002). In this context, the Parnaíba Delta displays a rather complex geomorphology (Fig. 1). The lowermost part of the main eastern distributary channel features several low-sinuosity bends and anastomosing bifurcation patterns. In the west, three NW–SE-oriented tidal channels drain a large mangrove area, which extends up to the more elevated mainland in the south. The delta thus has an asymmetric, wave- and tide-dominated shape (cf. Galloway 1975; Bhattacharya and Giosan 2003). Such deltas are typically associated with variable proportions of river-, wave- and tide-dominated facies among and within their lobes, the latter being characterized by morphological asymmetry between their downdrift and updrift sides, a feature also observed in the Parnaíba Delta. The littoral drift is directed westward (Bittencourt et al. 2005) and is responsible for sediment drift and spit development in that direction, although the mouths of both distributaries (Parnaíba and Igaraçu) are orientated SW–NE.

The eastern delta lobe is dominantly shaped by wave forcing from the northeast, almost perpendicular to the river mouth. As a consequence, the sedimentary facies and structures (lamination and lenticular bedding) in core VC03 indicate only moderate tidal influence in this area. The transgressive, southwestward migrating dune fields situated close to the shore reflect the main wind direction. Waves propagating in the same direction resuspend sediment in the nearshore zone, which is then transported toward the shore by residual wave drift and tidal currents to feed the delta front, as also observed on the Amazon shelf by Kuehl et al. (1985). Due to the slight drop in the post-5,000 year BP relative sea level in the region (Caldas et al. 2006a), the supply of sediment to the coast increased and contributed to both delta and dune field growth.

In the abandoned western delta lobe, the intricate mangrove tidal channel system (Fig. 1) is an indicator of increased tidal influence (cf. Galloway 1975), a feature also described by Knoppers et al. (1999) and which includes a main ebb channel, small ebb deltas, marginal flood channels and inlets with back-barrier channel systems, as well as tidal flats (cf. Flemming 2012). Several sand spits reveal the west–northwest longshore current direction. Tidal to lagoonal conditions are evidenced by the sedimentary facies and structure of cores VC08 and VC10 (lamination, flaser bedding, and cross-bedding).

Based on the modern delta configuration, the questions remain whether a natural connection between the western tidal channels and the main Parnaíba River distributary existed in former times, and how the specific configuration of the modern delta developed. The relative influences of river flow, tides and waves can change over time (Correggiari et al. 2005), as a consequence of which a tide-dominated system can switch to a wave-dominated system, and vice versa (Syvitski and Saito 2007), due to changes in sediment supply as well as wave or tidal forcing. A comparison of satellite images (Fig. 1) and old maps (Fig. 6) documents a change in the shape of the delta and the river mouth in recent times. The map of Heck (1842) shows a northwest orientation of the principal distributary, which splits into several river-mouth channels in the western delta lobe. The map of Walle (1910), by contrast, shows the main Parnaíba distributary in its modern position, but with smaller channels still connecting to the large channels of the formerly active western lobe. All these smaller channels are today abandoned, except for one that was reopened by human activity about 50 years ago (communication of local inhabitants). The two maps illustrate that delta lobe switching took place within a few decades between the two dates, and that natural connections between the western tidal channels and the main river distributary persisted for some time before becoming blocked in favor of the new distributary in the east. Similar processes have been described in the literature for other rivers such as the Brahmaputra, the Mississippi and the Yellow River (e.g., Roberts 1998; Chu et al. 2006; Pickering et al. 2014).

Tectonic influences

Fault reactivation might have occurred long after the rifting and early opening of the South Atlantic Ocean, and may therefore also have affected depositional processes in the Quaternary (Azevedo 1991). The Mesozoic rifting generated extensional and strike-slip faulting along the Brazilian equatorial margin (e.g., Szatmari et al. 1987; Almeida-Filho et al. 2009). Almeida-Filho et al. (2009) argued that the reactivation of the Pirapemas lineament, which is situated west of the Parnaíba Delta (Fig. 7), triggered a set of strike-slip movements in the area, which had an important influence on the sedimentation pattern and landscape evolution during the late Quaternary. A dextral strike-slip displacement along the Sobradinho fault on the border of the Sobradinho platform (Fig. 7) was observed on gravity maps. The area west of the Pirapemas lineament is characterized by valley incision and rectangular drainage patterns controlled by joints and faults (Almeida-Filho et al. 2009). The drainage channels east of the Pirapemas lineament, which extend to the Parnaiba Delta in the east, are mostly straight with flow direction toward the NE and connecting at high angles. The morphology and shape of the Parnaíba Delta has thus developed not only through coastal processes associated with river discharge and tidal and wave forcing, but also with neotectonic movements that caused tilting toward the east, and which may actually have initiated
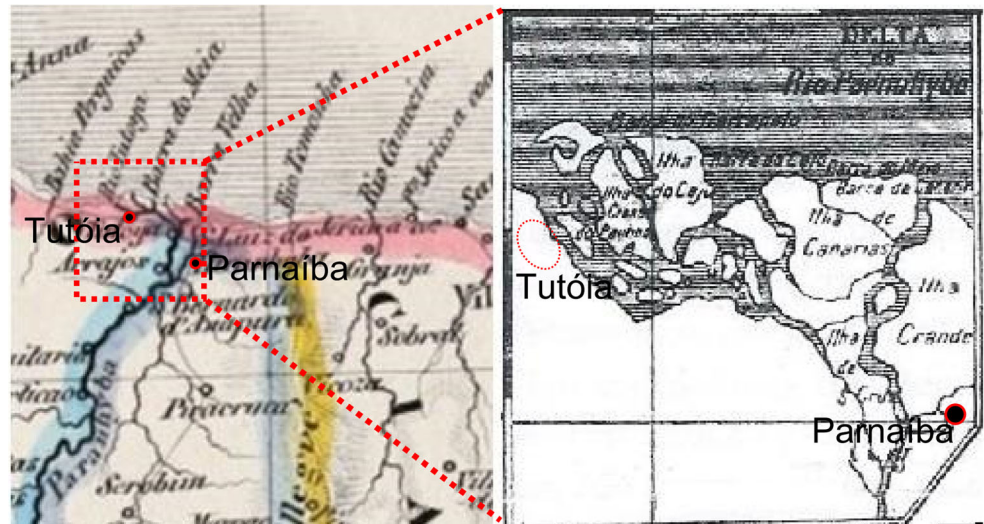
the delta lobe switching process. This can explain the erosional character of the main distributary near the river mouth and its unusual updrift orientation.

Interpretation of carbon and nitrogen signatures

C_{org}/N_{tot} and $\delta^{13}C$ signatures are widely accepted proxies serving to reconstruct the evolution of ancient coastal settings (e.g., Müller and Mathesius 1999; Bouillon et al. 2003, 2008; Lamb et al. 2006; Perdue and Koprivnjak 2007; Bianchi et al. 2007; Da Cruz Miranda et al. 2009; Leipe et al. 2011; Giresse et al. 2014), including major deltas such as that of the Mississippi (e.g., Rosenbauer et al. 2009). Figure 8 combines the present datasets with the typical ranges compiled by Lamb et al. (2006) for organic input to coastal environments worldwide. The $\delta^{13}C$ values of all cores combined span a narrow range between –23.57 and –27.10‰ (except for –21.08‰ recorded in core VC01 at 1 cm depth, Fig. 5), whereas the C_{org}/N_{tot} ratios span a wide range of ca. 15–50. All data points

plot within the range of terrestrial C_3 plants, and are consistent with findings for mangrove ecosystems worldwide (e.g., Dehairs et al. 2000; Jennerjahn and Ittekkot 2002; Bouillon et al. 2003, 2008). An unambiguous link of these signatures to the recent lobe switching of the Parnaíba Delta discussed above is not straightforward, for one because of limitations of stable isotope signatures (see Bouillon et al. 2008). A more meaningful approach would be to combine those data with independent observations of sediment facies, delta configuration on satellite images and historical maps, and the regional tectonic influence on depositional processes.

In core VC10, the lower C_{org}/N_{tot} ratios could plausibly be explained by a stronger influence of marine plants during sediment deposition (see Perdue and Koprivnjak 2007). In the present case, however, the lower $\delta^{13}C$ values rather
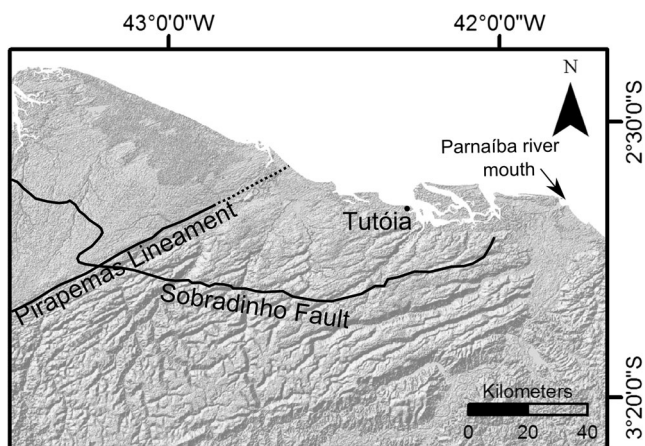

Fig. 7 Pirapemas lineament and drainage pattern along the eastern coast of Marañhao (modified from Azevedo 1991; Almeida-Filho et al. 2009)
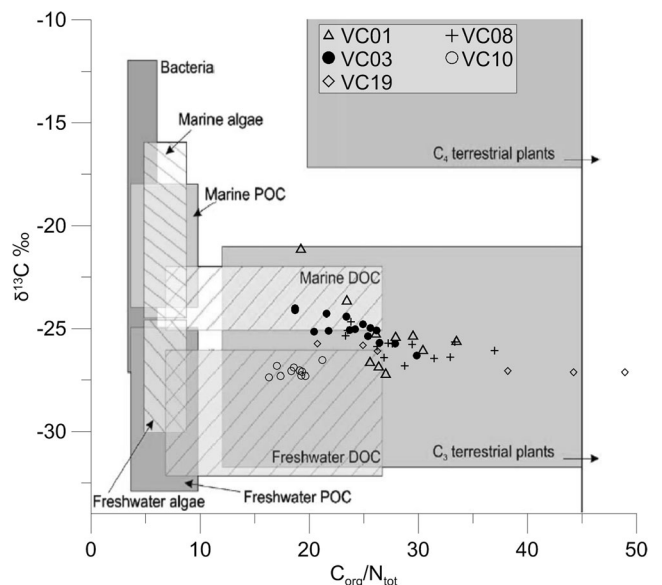

Fig. 8 Environmental significance of $\delta^{13}C$ versus C_{org}/N_{tot} (modified from Lamb et al. 2006)

suggest an input of freshwater DOC (dissolved organic carbon) and terrestrial plants from the nearby hinterland, although the bulk seems to be influenced by a mixture of marine and terrestrial input. The values are better clustered than those of the other cores (Fig. 8), a feature attributed to the young age. For the last 16 years, the environment and the source of carbon did not change as much as in the longer and older time periods covered by the other cores, especially core VC19.

Core VC19 features a marked decrease in the C_{org}/N_{tot} ratio from top to bottom (Fig. 5). The sediment of this core is older than that of the other cores, and the values of the six measured samples, which reflect environmental changes in the period 4, 400–4,200 cal. years BP, represent the longest period of deposition. The high C_{org}/N_{tot} ratios in the uppermost samples suggest that the terrestrial influence was highest in this part of the core, probably reflecting a progressive increase in river input from the hinterland in the course of time.

In core VC08, the low N_{tot} contents are an indication of terrestrial plant influence during deposition (e.g., Lamb et al. 2006) and therefore a stronger signal of the Parnaíba River. The clear distinction between cores VC08 and VC10 in the plot of Fig. 8 reflects changes between present and ancient conditions in the tidal-channel system. The change toward marine conditions in core VC10 was most likely generated by variations in river flow caused by the switching of distributary channels in the Parnaíba Delta, as demonstrated by the old maps and supported by the neotectonic influence on deposition. The higher river influence during deposition at the VC08 core site is more consistent with the cores taken from the eastern delta lobe than with the more recent tidal-marine conditions reflected in core VC10.

Conclusions

Present-day morphodynamic characteristics combined with grain-size, $\delta^{13}C$ and C_{org}/N_{tot} assessments have enabled reconstruction of the mid- to late-Holocene evolution of the pristine Parnaíba Delta spanning the last 5,000 years. Prevailing NE winds, SW-directed waves and westward-flowing longshore currents result in intense shoreward sediment transport and the formation of mobile transgressive dune fields. These conditions were responsible for the formation of an asymmetric wave- and tide-dominated delta.

The findings suggest that the western tidal-channel system is associated with an abandoned lobe of the Parnaíba Delta that was connected to the Parnaíba River in ancient times. The evolution of the former river-fed, tide-dominated western distributary channels into the present-day isolated tidal channels, and the switch of the river to the modern distributary in the east is substantiated by three arguments: (1) evaluation of $\delta^{13}C$, C_{org} and N_{tot} data shows a decrease of fluvial influence

in the young sediments of the tidal-channel area; (2) maps from the 19th and even early 20th Century provide evidence of a former natural connection between the main Parnaíba River distributary and the tidal channels to the west of the modern Parnaíba Delta; (3) the tectonic interpretation of satellite images establishes a link between the present-day asymmetric delta configuration, an eastward tilting and the initiation of delta lobe switching that resulted in the unusual updrift orientation of the main Parnaíba distributary. The comparison of old maps, satellite images and morphodynamics confirms the interpretation that delta lobe switching is still ongoing, an aspect deserving continued attention.

References

Alexander CR, Nittrouer CA, Demaster DJ, Park Y-A, Park S-C (1991) Macrotidal mudflats of the southwestern Korean coast; a model for interpretation of intertidal deposits. J Sed Res 61:805–824

Almeida-Filho R, Rossetti DF, Miranda FP, Ferreira FJ, Silva C, Beisl C (2009) Quaternary reactivation of a basement structure in the Barreirinhas Basin, Brazilian Equatorial Margin. Quat Res 72:103–110

ANA (2013) Agencia Nacional de Águas. http://www2.ana.gov.br/Paginas/portais/bacias/Parnaiba.aspx, accessed 6 May 2014

Angulo RJ, Lessa GC, Souza MC (2006) A critical review of mid- to late-Holocene sea-level fluctuations on the eastern Brazilian coastline. Quat Sci Rev 25:486–506

Arora B, Padilha A, Vitorello Í, Trivedo N, Fontes S, Rigoti A, Chamalaun F (1999) 2-D geoelectrical model for the Parnaíba Basin conductivity anomaly of northeast Brazil and tectonic implications. Tectonophysics 302:57–69

Azevedo RP (1991) Tectonic evolution of Brazilian equatorial continental margins. PhD Thesis, Royal School of Mines, Imperial College, London

Bartholomä A, Flemming BW (2007) Progressive grain-size sorting along an intertidal energy gradient. Sed Geol 202(3):464–472. doi:10.1016/j.sedgeo.2007.03.010

Bezerra FH, Barreto AM, Suguio K (2003) Holocene sea-level history on the Rio Grande do Norte State coast, Brazil. Mar Geol 196:73–89

Bhattacharya JP, Giosan L (2003) Wave-influenced deltas: geomorphological implications for facies reconstruction. Sedimentology 50:187–210

Bianchi TS, Galler JJ, Allison MA (2007) Hydrodynamic sorting and transport of terrestrially derived organic carbon in sediments of the Mississippi and Atchafalaya Rivers. Estuar Coastal Shelf Sci 73:211–222

da SP Bittencourt AC, Dominguez JML, Martin L, Silva IR (2005) Longshore transport on the northeastern Brazilian coast and implications to the location of large scale accumulative and erosive zones: an overview. Mar Geol 219:219–234

Bittencourt ACDSP, Dominguez JML, Fontes LCS, Sousa DL, Silva IR, da Silva FR (2007) Wave refraction, river damming, and episodes of severe shoreline erosion: the São Francisco river mouth, Northeastern Brazil. J Coastal Res 23(4):930–938

Bouillon S, Dahdouh-Guebas F, Rao AVVS, Koedam N, Dehairs F (2003) Sources of organic carbon in mangrove sediments: variability and possible ecological implications. Hydrobiologia 495:33–39

Bouillon S, Connolly RM, Lee SY (2008) Organic matter exchange and cycling in mangrove ecosystems: recent insights from stable isotope studies. J Sea Res 59:44–58

de Oliveira Caldas LH, Stattegger K, Vital H (2006a) Holocene sea-level history: evidence from coastal sediments of the northern Rio Grande do Norte coast, NE Brazil. Mar Geol 228:39–53

de Oliveira Caldas LH, de Jr Oliveira JG, de Medeiros WE, Stattegger K, Vital H (2006b) Geometry and evolution of Holocene transgressive and regressive barriers on the semi-arid coast of NE Brazil. Geo-Mar Lett 26:249–263

CHESF (2014) Companhia Hidro Elétrica do São Francisco. http://www.chesf.gov.br/portal/page/portal/chesf_portal/paginas/sistema_chesf/sistema_chesf_geracao/conteiner_geracao?p_name=8A2EEABD3BDDD002E0430A803301D002, accessed 11 March 2014

Chu ZX, Sun XG, Zhai SK, Xu KH (2006) Changing pattern of accretion/erosion of the modern Yellow River (Huanghe) subaerial delta, China: based on remote sensing images. Mar Geol 227:13–30

Correggiari A, Cattaneo A, Trincardi F (2005) The modern Po Delta system: lobe switching and asymmetric prodelta growth. Mar Geol 222(223):49–74

Costa JBS, Hasui Y, Bemerguy RL, Soares-Júnior AV, Villegas JMC (2002) Tectonics and paleogeography of the Marajó Basin, northern Brazil. Anais Acad Bras Ciências (Annals Braz Acad Sci) 74:519–531

Da Cruz Miranda MC, De Fátima Rossetti D, Carlos Ruiz Pessenda L (2009) Quaternary paleoenvironments and relative sea-level changes in Marajó Island (Northern Brazil): facies, δ^{13}C, δ^{15}N and C/N. Palaeogeogr Palaeoclimatol Palaeoecol 282:19–31

Dehairs F, Rao RG, Mohan PC, Raman AV, Maguillier S, Hellings L (2000) Tracing mangrove carbon in suspended matter and aquatic fauna of the Gautami–Godavari Delta, Bay of Bengal (India). Hydrobiologia 431:225–241

Dominguez JML (2009) The coastal zone of Brazil. In: Dillenburg S, Hesp P (eds) Geology and geomorphology of Holocene coastal barriers of Brazil. Springer, Heidelberg, pp 17–51

Fan D (2012) Open-coast tidal flats. In: Davis RA, Dalrymple RW (eds) Principles of tidal sedimentology. Springer, Heidelberg, pp 187–229

Flemming BW (2012) Siliciclastic back-barrier tidal flats. In: Davis RA, Dalrymple RW (eds) Principles of tidal sedimentology. Springer, Heidelberg, pp 231–267

Folk RL (1954) The distinction between grain size and mineral composition in sedimentary-rock nomenclature. J Geol 62:344–359

Frey RW, Howard JD, Han S-J, Park B-K (1989) Sediments and sedimentary sequences on a modern macrotidal flat, Inchon, Korea. J Sed Res 59:28–44

Galloway WE (1975) Process framework for describing the morphologic and stratigraphic evolution of deltaic depositional systems. In: Broussard ML (ed) Deltas: models for exploration. Houston Geological Society, Houston, pp 87–98

Giresse P, Pascucci V, Lymer G, Gaullier V, Thinon I (2014) Processes controlling very low sedimentation rates on the continental slope of the Gonone-Orosei canyon system, NE Sardinia—terrestrial and oceanic significance. Geo-Mar Lett 34:483–498

Heck (1842) Brazil Empire Rio de Janeiro original historical old map. http://www.mapandmaps.com/de/sudamerika/1744-brazil-empire-rio-de-janeiro-original-historical-old-map-heck-1842.html, accessed 4 April 2014

Hesp PA, Maia LP, Claudino-Sales V (2009) The Holocene barriers of Maranhão, Piauí and Ceará, Northeastern Brazil. In: Dillenburg S, Hesp P (eds) Geology and geomorphology of Holocene coastal barriers of Brazil. Springer, Heidelberg, pp 325–345

Irion G, de Morais JO, Bungenstock F (2012) Holocene and Pleistocene sea-level indicators at the coast of Jericoacoara, Ceará, NE Brazil. Quat Res 77(2):251–257

Jaffe BE, Smith RE, Foxgrover AC (2007) Anthropogenic influence on sedimentation and intertidal mudflat change in San Pablo Bay, California: 1856–1983. Estuar Coastal Shelf Sci 73:175–187

Jennerjahn TC, Ittekkot V (2002) Relevance of mangroves for the production and deposition of organic matter along tropical continental margins. Naturwissenschaften 89:23–30

Knoppers B, Ekau W, Figueiredo AG (1999) The coast and shelf of east and northeast Brazil and material transport. Geo-Mar Lett 19:171–178

Kuehl SA, Nittrouer CA, DeMaster DJ (1985) Distribution of sedimentary structures in the Amazon subaqueous delta. Cont Shelf Res 6:311–336

Labohidro (1999) Diagnóstico ambiental da Ilha do Caju. Relatório sintese das unidades ambientais. Universidade Federal do Maranhão, Maranhão

Lamb AL, Wilson GP, Leng MJ (2006) A review of coastal palaeoclimate and relative sea-level reconstructions using δ^{13}C and C/N ratios in organic material. Earth Sci Rev 75:29–57

Lanesky DE, Logan BW, Brown RG, Hine AC (1979) A new approach to portable vibracoring underwater and on land. J Sed Petrol 49:665–657

Leipe T, Tauber F, Vallius H, Virtasalo J, Uścinowicz S, Kowalski N, Hille S, Lindgren S, Myllyvirta T (2011) Particulate organic carbon (POC) in surface sediments of the Baltic Sea. Geo-Mar Lett 31:175–188

Lo EL, Bentley SJ Sr, Xu K (2014) Experimental study of cohesive sediment consolidation and resuspension identifies approaches for coastal restoration: Lake Lery, Louisiana. Geo-Mar Lett 34:499–509

Marques M, da Costa MF, de O Mayorga MI, Pinheiro PRC (2004) Water environments: anthropogenic pressures and ecosystem changes in the Atlantic drainage basins of Brazil. J Human Environ 33(1):68–77

Martinez JM, Guyot JL, Filizola N, Sondag F (2009) Increase in suspended sediment discharge of the Amazon River assessed by monitoring network and satellite data. Catena 79:257–264

Müller A, Mathesius U (1999) The palaeoenvironments of coastal lagoons in the southern Baltic Sea, I. The application of sedimentary C_{org}/N ratios as source indicators of organic matter. Palaeogeogr Palaeoclimatol Palaeoecol 145:1–16

Nimer E (1979) Climatology of Brazil (in Portuguese). Série Recursos Naturais e Meio Ambiente, vol 4. SUPREN/IBGE, Rio de Janeiro

Nittrouer CA, Sternberg RW, Carpenter R, Bennett JT (1979) The use of Pb-210 geochronology as a sedimentological tool: application to the Washington continental shelf. Mar Geol 31:297–316

Perdue EM, Koprivnjak J-F (2007) Using the C/N ratio to estimate terrigenous inputs of organic matter to aquatic environments. Estuar Coastal Shelf Sci 73:65–72

Pickering JL, Goodbred SL, Reitz MD, Hartzog TR, Mondal DR, Hossain MS (2014) Late Quaternary sedimentary record and Holocene channel avulsions of the Jamuna and Old Brahmaputra River valleys in the upper Bengal delta plain. Geomorphology 227:123–136. doi:10.1016/j.geomorph.2013.09.021

Reimer PJ, Bard E, Bayliss A, Beck JW, Blackwell PG, Ramsey CB, Buck CE, Cheng H, Edwards RL, Friedrich M, Grootes PM, Guilderson TP, Haflidason H, Hajdas I, Hatté C, Heaton TJ, Hoffmann DL, Hogg AG, Hughen KA, Kaiser KF, Kromer B, Manning SW, Niu M, Reimer RW, Richards DA, Scott EM, Southon JR, Staff RA, Turney CSM, van der Plicht J (2013) IntCal13 and Marine13 Radiocarbon Age Calibration Curves 0–50,000 Years cal BP. Radiocarbon 55:1869–1887

Reineck HE, Singh IB (1975) Depositional sedimentary environments. Springer, Berlin

Roberts HH (1998) Delta switching: early responses to the Atchafalaya River Diversion. J Coastal Res 14(3):882–899

Rosenbauer RJ, Swarzenski PW, Kendall C, Orem WH, Hostettler FD, Rollog ME (2009) A carbon, nitrogen, and sulfur elemental and isotopic study in dated sediment cores from the Louisiana Shelf. Geo-Mar Lett 29:415–429

Schäfer A (2005) Klastische Sedimente: Fazies und Sequenzstratigraphie. Elsevier, München

Stuiver M, Polach HA (1977) Discussion: Reporting of ^{14}C Data. Radiocarbon 19(3):355–363

Suguio K, Martin L (1981) Significance of Quaternary sea-level fluctuations for delta construction along the Brazilian coast. Geo-Mar Lett 1:181–185

Syvitski JPM, Saito Y (2007) Morphodynamics of deltas under the influence of humans. Global Planet Change 57:261–282

Syvitski JPM, Kettner AJ, Overeem I, Hutton EWH, Hannon MT, Brakenridge GR, Day J, Vörösmarty C, Saito Y, Giosan L, Nicholls RJ (2009) Sinking deltas due to human activities. Nature Geosci 2:681–686

Szatmari P, Batista J, Françolin L, Zanotto O, Wolf S (1987) Evolução tectônica da margem equatorial brasileira. Rev Bras Geociências 17:180–188

Szlafsztein CF (2003) Vulnerability and response measures to natural hazard and sea level rise impacts: long term coastal zone management, NE of the State of Pará, Brazil. PhD Thesis, Christian-Albrechts-Universität zu Kiel, Kiel

Traini C, Schrottke K, Stattegger K, Dominguez JML, Guimarães JK, Vital H, d'Avila Beserra D, da Silva Aquino AG (2012) Morphology of subaqueous dunes at the mouth of the dammed River São Francisco (Brazil). J Coastal Res 28(6):1580–1590

Walle P (1910) No Brasil do Rio São Francisco ao Amazonas. Edicoes do Senado Federal 71, Brasilia 2006, pp 237–290

Walsh J, Nittrouer C (2004) Mangrove-bank sedimentation in a mesotidal environment with large sediment supply, Gulf of Papua. Mar Geol 208:225–248

Woodroffe CD (2002) Coasts. Form, process and evolution. Cambridge University Press, Cambridge

Wright LD, Coleman JM (1973) Variation in morphology of major river deltas as function of ocean wave and river discharge regimes. AAPG Bull 57:370–398

Zaborska A, Carroll J, Papucci C, Pempkowiak J (2007) Intercomparison of alpha and gamma spectrometry techniques used in ^{210}Pb geochronology. J Environ Radioactiv 93:38–50